An analytical solution of convective heat transfer in microchannel or nanochannel

Qiangqiang Sun, Kwing-So Choi, Xuerui Mao

Faculty of Engineering, University of Nottingham, Nottingham, NG7 2RD, UK.

Abstract

The two-dimensional energy equation with a first-order velocity slip model and a temperature jump model is studied analytically and a solution consisting of an infinite series is obtained. Impacts of viscous dissipation, axial conduction and rarefied effect on the local Nusselt number, the asymptotic Nusselt number and the bulk temperature profile of fluid are investigated. Results show that the cooling effect of the fluid benefits from the higher rarefied effect and axial conduction effect, as well as the lower viscous dissipation. The asymptotic dimensionless bulk temperature of fluid converges to a constant value that is higher than the wall temperature at a given set of Brinkman number, Péclet number and Knudsen number regardless of the inlet conditions. When neglecting axial conduction and the rarefied effect, the asymptotic Nusselt number with or without viscous dissipation is 17.5 or 7.54, respectively. Effects of axial conduction on the asymptotic Nusselt number are negligible when the Péclet number is greater than 10, while its influence on the non-dimensional bulk temperature of fluid and local Nusselt number can be neglected only when $Pe > 100$.

Keywords:
Axial conduction, Viscous dissipation, Péclet number, Brinkman number, Knudsen number

1. Introduction

Heat transfer in microchannel or nanochannel has drawn significant attention due to the rapid development of micromechanics in the last decades and its engineering applications in film cooling [1–4]. Experiments have shown that flow and heat transfer characters in microchannel or nanochannel are quite different from their well-known macroscale counterparts [5, 6]. Particularly, axial conduction and viscous dissipation which are generally neglected in macroscale flow and heat transfer problems are not trivial in microscale or nanoscale heat transfer due to the following factors: (1) No-slip velocity, no-slip temperature boundary conditions and even the continuum assumption widely used in macrochannel fluid flow and heat transfer governing equations become less valid as the size of channel is reduced. (2) In microchannel or nanochannel, the molecular mean free path is in the same order as that of channel size, which requires the consideration of molecular effects on heat transfer.

Significant efforts have been devoted to studying the effect of viscous dissipation. Tso et al. [7–9] performed dimensional analyses and experiments to show the impact of Brinkman number on the microchannel flow. Their results stated that the Brinkman number has an essential role in determining the flow transition point and the temperature distribution in spite of its relatively small values. Tunc et al. [10] studied the effect of viscous dissipation on the heat transfer of microtubes with uniform temperature and uniform heat flux via the integral transform technique and they obtained the asymptotic Nusselt number at prescribed Knudsen number, Brinkman number and Prandtl number. The same authors [11] also applied the H2-type boundary condition to analyze viscous dissipation influences on the temperature field in a rectangular channel at constant axial and wall normal heat flux and obtained similar results as in circular microtubes. Koo et al. [12] used dimensional analyses and numerical simulations to reveal effects of viscous dissipation on the temperature profile and friction factor for three working fluids (water, methanol and isopropanol) with various conduit geometries and showed that viscous dissipation cannot be neglected in flow in micro conduits.

A series of analytical solutions for heat transfer in

Nomenclature:

A_n	summation coefficients	z_n	variable in confluent hypergeometric function
a_n	coefficients in confluent hypergeometric function	**Greek symbols**	
Br	Brinkman number, $Br = \frac{\mu u_{ave}^2}{k(T_i - T_w)}$	α	thermal diffusivity
b_n	coefficients in confluent hypergeometric function	β_n	eigenvalues
C_1	$\frac{2-\sigma_t}{\sigma_t}\frac{2\gamma}{\gamma+1}\frac{Kn}{Pr}$	γ	specific heat ratio, $\gamma = 1.4$
C_2	$1 + 12\frac{2-\sigma}{\sigma}Kn$	λ	molecular mean free path
c_p	specific heat	μ	dynamics viscosity
D_H	hydraulic diameter of a 2D channel, $D_H = 4H$	θ	dimensionless temperature, $\theta = \frac{T-T_w}{T_i-T_w}$
$f_n(\eta)$	eigenfunctions	ρ	fluid density
$g_n(z_n)$	confluent hypergeometric function	ξ	dimensionless coordinate, $\xi = \frac{x}{Re \cdot Pr \cdot H}$
h	heat transfer coefficient	η	dimensionless coordinate, $\eta = \frac{y}{H}$
H	half of the channel height	σ	tangential momentum coefficient, $\sigma = 1$
k	thermal conductivity	σ_T	thermal accommodation coefficient, $\sigma_T = 1$
Kn	Knudsen number, $Kn = \frac{\lambda}{D_H}$	δ	relative difference
k_1	$\frac{3}{C_2}\frac{2-\sigma}{\sigma}Kn$	**Subscripts**	
k_2	$\frac{3}{8C_2}$	ave	average value
N	number of eigenvalues or eigenfunctions	b	bulk value
Nu	Nusselt number, $Nu = \frac{hD_H}{k}$	c	critical value
Pe	Péclet number, $Pe = Re \cdot Pr = \frac{u_{ave}D_H}{\alpha}$	F	asymptotic value
Pr	Prandtl number, $Pr = \frac{\nu}{\alpha}$	i	inlet prperties
Re	Reynolds number, $Re = \frac{u_{ave}D_H}{\nu}$	L	local value
T	temperature	s	fluid properties at wall
u	velocity	w	wall properties
W	channel width	**Superscript**	
x, y	cartesian coordinate	$*$	non-dimensional value

one-dimensional microchannel when only axial conduction is considered has been extensively reported [13–20]. For example, Lahjomri et al. [14, 15] and Haji-Sheikh et al. [20] applied the series analysis solution method to investigate the temperature profile in parallel plate channels or circular ducts, respectively. They concluded that the effect of axial conduction influence needs to be considered when $Pe < 10$. Minkowycz et al. [19] also adopted this approach to analyze heat transfer in saturated porous passages. Both experimental and numerical simulation were applied by Tiselj et al. [17] to obtain axial conduction effects on heat transfer characters for water flow through a triangular channel at various Reynolds numbers. The wall temperatures obtained from these two methods have a good agreement and the local Nusselt number along the flow direction has a singular point whose location is a function of the Reynolds number. The bulk temperature of water exceeds the temperature of the heated wall after this singular point. Maranzana et al. [18] proposed two analytical models that were utilized to analyze the influence of axial conduction on the wall using a new non-dimensional number M ($M = \frac{\Phi_{cond//}}{\Phi_{conv}}$, $\Phi_{cond//}$ is wall axial heat flux and Φ_{conv} is the total convective heat flux.). They found that the wall heat flux density becomes quite non-uniform when the Reynolds number is small and the heat transfer coefficient for small flow rates may be underestimated when using experimental data with a one-dimensional model to measure this coefficient. Gu et al. [21] analyzed axial conduction impacts on convective heat transfer via the molecular dynamics simulation method and believed that its influence should be considered in the range of $Pe < 10$. However, Hennecke[22] stated that axial conduction might be neglected for the end of the domain in channels if $Pe > 20$.

Shah et al. [23] reviewed previous works on the joint effect of axial conduction and viscous dissipation on heat transfer in ducts. Nield et al. [24] investigated the effects of axial conduction and viscous dissipation on forced heat transfer in a porous medium with a constant temperature boundary condition and they obtained an analytical expression for the local Nusselt number as a function of non-dimensional numbers (Darcy number, Péclet number and Brinkman number). Hetsroni et al. [25] also considered viscous dissipation and axial conduction (on the fluid and the wall, jointly and separately.) effects on microtube hydrodynamics in asymptotic incompressible flow with constant physical properties via assuming $\frac{\partial T(x,y)}{\partial y} \approx 0$ (this means fluid temperature profile is 1D). In order to show the local Nusselt number distribution as a function of non-dimensional parameters (Knudsen number, Péclet number and Brinkman number), Jeong et al. [26] solved the 2D non-dimensional energy equation using a segregation variable method to make the dimensionless temperature equal to the sum of an asymptotic temperature θ_1 and another variable θ_2. The latter variable can be expanded as an infinite series of eigenfunctions. These eigenfunctions and their coefficients in the infinite series can be computed by invoking the shooting method and the Galerkin method, respectively. Nevertheless, the exact mathematical expression of temperature was not given. Cetin et al. [27] adopted first-order velocity slip model without a temperature jump in order to address the 2D energy equation of fluid flow in microtubes including viscous dissipation, axial conduction and rarefaction via a coordinate transformation approach [28, 29]. This may not precisely mimic convective heat transfer since fluid temperature jump is general in the vicinity of the wall. Barışık et al. [30] defined a non-dimensional coordinate system. Then, the energy equation was solved analytically in this new dimensionless coordinate system. It was found that, when the viscous dissipation is neglected, axial conduction effects need to be considered as the Péclet number is less than 100. Haddout et al. [31] decomposed the energy equation into a system of the first-order partial differential equations and then solved the latter in order to show the effects of axial conduction, viscous dissipation and pressure work on heat transfer of a gaseous slip flow. They indicated that the effects of axial conduction on heat transfer should be considered in the range of $Pe < 10$ as reported by [14, 15, 20, 21]. Clearly, a consensus for the axial conduction impacts on heat transfer has not been reached.

Unlike previous works reviewed above, in this study, viscous dissipation term and axial conduction term are considered simultaneously in the process of deriving the analytical solution of the 2D energy equation with the first-order velocity slip model and the temperature jump boundary model. We give the analytical expression of dimensionless 2D temperature profile via much simpler separation of variables and substitution approaches and apply it to examine the impacts of viscous dissipation, axial conduction and rarefied effect on heat transfer. Results indicate good cooling effects can be achieved via increasing Knudsen number, and reducing Brinkman number and Péclet number. Effects of axial conduction on asymptotic Nusselt number become less important when $Pe > 10$, while the impacts on local Nusselt number and bulk dimensionless temperature can be neglected only when $Pe > 100$. This clearly demonstrates the impact of axial conduction on heat transfer.

2. Analytical solution of the 2D energy equation

The geometry of the parallel plate microchannel or nanochannel considered in this paper and the flow chart of the analytical solution are shown in Fig. 1 and Fig. 2, respectively. Assuming that fluid property including

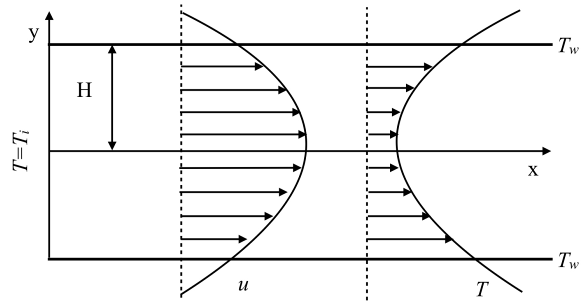

Figure 1: Definition sketch

density, specific heat, thermal conductivity and dynamic viscosity, are constants, the 2D energy equation including axial conduction and viscous dissipation, as well as boundary conditions can be established as

$$\rho c_p u \frac{\partial T}{\partial x} = k \frac{\partial^2 T}{\partial x^2} + k \frac{\partial^2 T}{\partial y^2} + \mu \left(\frac{\partial u}{\partial y} \right)^2, \tag{1}$$

$$T = T_i \qquad at \qquad x = 0, \tag{2a}$$

$$\frac{\partial T}{\partial y} = 0 \qquad at \qquad y = 0, \tag{2b}$$

$$T - T_w = -\frac{2 - \sigma_T}{\sigma_T} \frac{2\gamma}{\gamma + 1} \frac{\lambda}{Pr} \frac{\partial T}{\partial y} \qquad at \quad y = H. \tag{2c}$$

In Eq. (1), $\rho c_p u \frac{\partial T}{\partial x}$ is the convective term, and the three terms on the right side represent axial conduction, heat conduction normal to the wall and viscous dissipation, respectively. The first and second boundary condition in Eq. (2a) and Eq. (2b) are the uniform temperature at the channel entrance and symmetry temperature at the centreline, respectively. The third boundary condition shown in Eq. (2c) is the first-order temperature jump model derived from an energy balance at the wall by Kennard [32].

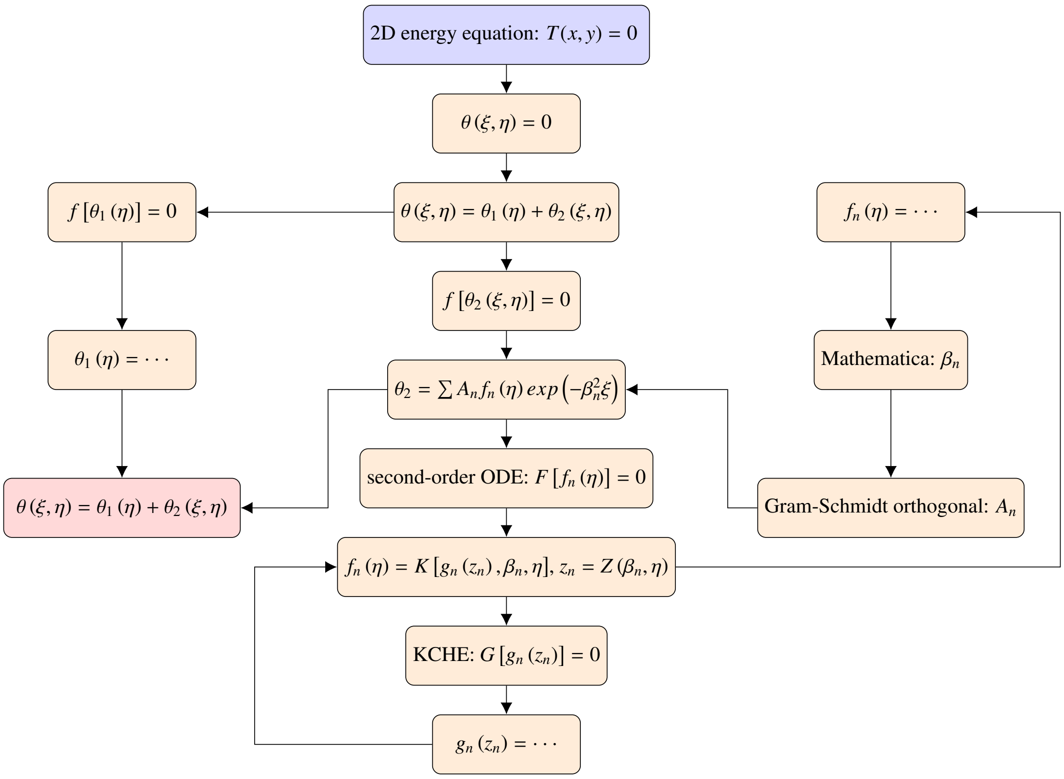

Figure 2: Flow chart of the analytical solution of the 2D energy equation (KCHE stands for the Kummer confluent hypergeometric equation).

We define the following dimensionless variables

$$\theta=\frac{T-T_w}{T_i-T_w},\qquad Br=\frac{\mu u_{ave}^2}{k\,(T_i-T_w)},$$
$$\xi=\frac{x}{Re\cdot Pr\cdot H},\qquad \eta=\frac{y}{H}. \tag{3}$$

The energy equation and boundary conditions can thus be non-dimensionalized as

$$\frac{1}{4}u^*\frac{\partial\theta}{\partial\xi}=\frac{1}{Pe^2}\frac{\partial^2\theta}{\partial\xi^2}+\frac{\partial^2\theta}{\partial\eta^2}+Br\left(\frac{\partial u^*}{\partial\eta}\right)^2, \tag{4}$$

$$\theta=1\qquad at\qquad \xi=0, \tag{5a}$$
$$\frac{\partial\theta}{\partial\eta}=0\qquad at\qquad \eta=0, \tag{5b}$$
$$\theta=-4C_1\frac{\partial\theta}{\partial\eta}\qquad at\quad \eta=1, \tag{5c}$$

where the non-dimensionless velocity u^* is given by [26]

$$u^*=\frac{u}{u_{ave}}=\frac{3}{2}\frac{1-\eta^2+8\frac{2-\sigma}{\sigma}Kn}{C_2}. \tag{6}$$

θ can be decomposed as an asymptotic temperature θ_1 ($\xi\to+\infty$) and a transient term

$$\theta=\theta_1+\theta_2. \tag{7}$$

When $\xi\to+\infty$, there is

$$\frac{\partial\theta_1}{\partial\xi}=0,\qquad \frac{\partial^2\theta_1}{\partial\xi^2}=0. \tag{8}$$

Subsequently, after substituting Eq. (7) and Eq. (8) into Eq. (4) and Eqs. (5a) to (5c), we obtain two sets of dimensionless energy equations and boundary conditions for θ_1 and θ_2

$$\frac{\partial^2\theta_1}{\partial\eta^2}=-Br\left(\frac{\partial u^*}{\partial\eta}\right)^2, \tag{9}$$

$$\frac{\partial\theta_1}{\partial\eta}=0\qquad at\qquad \eta=0, \tag{10a}$$
$$\theta_1=-4C_1\frac{\partial\theta_1}{\partial\eta}\qquad at\quad \eta=1, \tag{10b}$$

and

$$\frac{1}{4}u^*\frac{\partial\theta_2}{\partial\xi}-\frac{1}{Pe^2}\frac{\partial^2\theta_2}{\partial\xi^2}-\frac{\partial^2\theta_2}{\partial\eta^2}=0, \tag{11}$$

$$\frac{\partial \theta_2}{\partial \eta} = 0 \qquad at \qquad \eta = 0, \tag{12a}$$

$$\theta_2 = -4C_1 \frac{\partial \theta_2}{\partial \eta} \qquad at \quad \eta = 1. \tag{12b}$$

Through solving Eq. (9) with boundary conditions Eqs. (10a) and (10b), the asymptotic temperature θ_1 is obtained,

$$\theta_1 = \frac{Br}{C_2^2}\left(\frac{-3}{4}\eta^4 + \frac{3}{4} + 12C_1\right). \tag{13}$$

According to references [33–36], the solution θ_2 of the homogeneous partial differential Eq. (11) can be written as

$$\theta_2 = \sum_{n=1}^{\infty} A_n f_n(\eta) exp\left(-\beta_n^2 \xi\right). \tag{14}$$

In this infinite series, each term consists of a magnitude A_n, a function f_n and an exponential term depending on ξ. After substituting Eq. (14) into Eq. (11), Eq. (12a) and Eq. (12b), the following equation and boundary conditions can be obtained

$$\frac{d^2 f_n(\eta)}{d\eta^2} + \beta_n^2\left(\frac{1}{4}u^* + \frac{\beta_n^2}{Pe^2}\right) f_n(\eta) = 0, \tag{15}$$

$$\frac{d f_n(\eta)}{d\eta} = 0 \qquad at \qquad \eta = 0, \tag{16a}$$

$$f_n(\eta) = -4C_1 \frac{d f_n(\eta)}{d\eta} \qquad at \quad \eta = 1, \tag{16b}$$

where $f_n(\eta)$ and β_n are eigenfunctions and eigenvalues, respectively.

Now, we define two new variables

$$f_n(\eta) = exp\left(\frac{-1}{2}\beta_n \sqrt{k_2}\eta^2\right) g_n(z_n), \tag{17a}$$

$$z_n = \beta_n \sqrt{k_2}\eta^2. \tag{17b}$$

With the dimensionless velocity in Eq. (6), boundary condition in Eq. (16a) and variable transformation in Eqs. (17a) and (17b), Eq. (15) can be reformulated as

$$z_n \frac{d^2 g_n(z_n)}{dz_n^2} + \left(\frac{1}{2} - z_n\right)\frac{dg_n(z_n)}{dz_n} - g_n(z_n)\cdot \frac{-\beta_n^3 - k_1 Pe^2\beta_n - k_2 Pe^2 \beta_n + Pe^2\sqrt{k_2}}{4Pe^2\sqrt{k_2}} = 0. \tag{18}$$

Eq. (18) is the standard confluent hypergeometric equation, whose solution can be expressed as

$$g_n(z_n) = {}_1F_1(a_n, b_n; z_n) = \sum_{m=0}^{\infty} \frac{(a_n)^{(m)}(z_n)^m}{(b_n)^{(m)} m!}, \tag{19}$$

where ${}_1F_1(a_n, b_n; z_n)$ is the confluent hypergeometric function [37] and a_n and b_n are

$$a_n = \frac{-\beta_n^3 - k_1 Pe^2\beta_n - k_2 Pe^2\beta_n + Pe^2\sqrt{k_2}}{4Pe^2\sqrt{k_2}}, \qquad b_n = \frac{1}{2}. \tag{20}$$

After substituting Eq. (19) into Eq. (17a), the eigenfunctions $f_n(\eta)$ become

$$f_n(\eta) = exp\left(\frac{-1}{2}\beta_n \sqrt{k_2}\eta^2\right)\sum_{m=0}^{\infty} \frac{(a_n)^{(m)}(z_n)^m}{(b_n)^{(m)} m!}. \tag{21}$$

These eigenvalues β_n can be determined via applying the boundary condition in Eq. (16b).

Therefore, θ_2 in Eq. (14) can be calculated from

$$\theta_2 = \sum_{n=1}^{\infty} A_n \left[\sum_{m=0}^{\infty} \frac{(a_n)^{(m)}(z_n)^m}{(b_n)^{(m)} m!} exp\left(\frac{-1}{2}\beta_n\sqrt{k_2}\eta^2\right)\right]\cdot exp\left(-\beta_n^2\xi\right), \tag{22}$$

where a_n, b_n, and z_n are shown in Eq. (20) and Eq. (17b), respectively.

Substituting Eq. (22) and Eq. (13) into Eq. (7), we can obtain

$$\theta = \frac{Br}{C_2^2}\left(\frac{-3}{4}\eta^4 + \frac{3}{4} - 12C_1\right) + \sum_{n=1}^{\infty} A_n \cdot \left[\sum_{m=0}^{\infty} \frac{(a_n)^{(m)}(z_n)^m}{(b_n)^{(m)} m!} exp\left(\frac{-1}{2}\beta_n\sqrt{k_2}\eta^2\right)\right] exp\left(-\beta_n^2\xi\right). \tag{23}$$

The summation constants A_n may be obtained from the boundary condition in Eq. (5a) by using the Gram-Schmidt orthogonal approach which is illustrated in detail in Appendix A. The algorithm of this method is outlined in Appendix B.

Once unknown eigenvalues β_n and summation coefficients A_n are determined, we can obtain the dimensionless temperature θ in the microchannel or nanochannel. The dimensionless bulk temperature θ_b for fluid flow through the parallel channel and the local Nusselt number which is the ratio of convective to conductive heat transfer normal to the wall boundary can be calculated from following equations, respectively:

$$\theta_b(\xi) = \int_0^1 u^*(\eta)\,\theta(\xi,\eta)\, d\eta, \tag{24}$$

$$Nu_L = \frac{hD_H}{k} = -\frac{4}{\theta_b(\xi)}\frac{\partial\theta(\xi,\eta)}{\partial\eta}\bigg|_{\eta=1}. \tag{25}$$

The bulk temperature T_b for fluid is

$$\begin{aligned} T_b(x) &= \frac{\int_0^H \rho u(y) W c_p T(x,y)\, dy}{\int_0^H \rho u(y) W c_p\, dy} \\ &= \frac{\int_0^H u(y) T(x,y)\, dy}{\int_0^H u(y)\, dy} \\ &= \frac{1}{Hu_{ave}}\int_0^H u(y) T(x,y)\, dy \\ &= \frac{1}{H}\int_0^H u^*(y) T(x,y)\, dy. \end{aligned} \tag{26}$$

3. Validation of the analytical solution

The infinite series in Eq. (22) can be truncated to the first N terms to approximate the non-dimensional temperature θ_2 with the reduced computational cost. At $N = 20$, the dimensionless bulk temperature can be converged to 5 significant figures. Then $N = 20$ is used in the following sections, the same as adopted in references [30, 36].

Then, we compare our results with those of Jeong et al. [26] to validate the accuracy of our non-dimensional analytical solution of the energy equation. After substituting the first 20 eigenvalues and summation coefficients determined via using the Gram-Schmidt orthogonal approach (*see AppendixB*) into Eq. (25) and Eq. (24), the rarefied effect on local Nusselt and how viscous dissipation affects the fluid bulk temperature distribution are shown in Fig. 3 and Fig. 4, respectively. It can be seen that our results are in excellent agreement with the reference [26].

In addition to that, we also redefine non-dimensional variables and re-address the dimensionless energy equation in literature [30]. The asymptotic Nusselt number at $\widetilde{Pe} = 1.0, Kn = 0, Br = 0$ computed using the present approach is 4.0273, which is nearly equal to 4.027 from the reference [30].

All comparisons, therefore, indicate that our non-dimensional analytical solution has sufficient accuracy. In the following section, this approach is utilized to analyze how viscous dissipation, axial conduction and rarefied affect heat transfer characteristics.

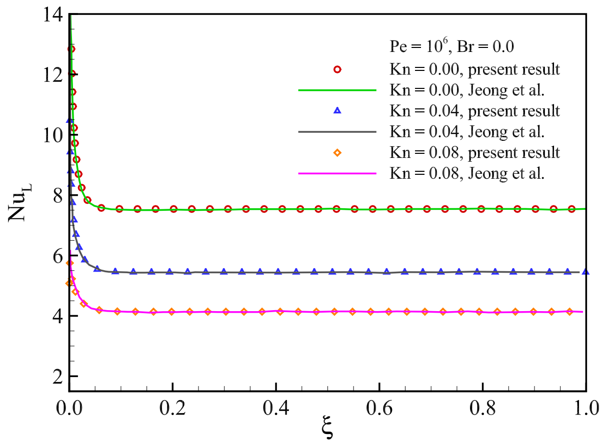

Figure 3: Effects of rarefied on local Nusselt number when axial conduction and viscous dissipation are neglected.

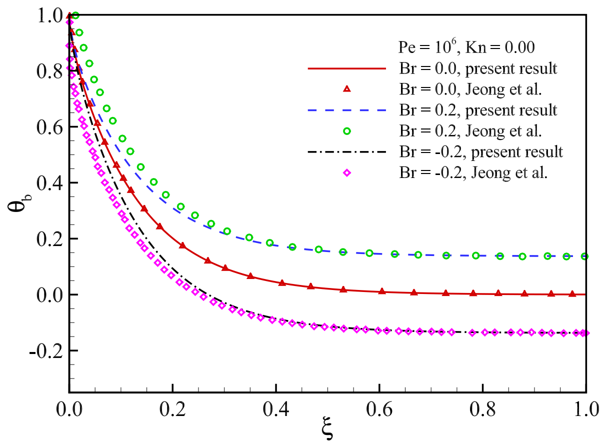

Figure 4: Viscous dissipation effects on fluid bulk temperature.

4. Results on the overshoot of fluid temperature

The key finding of the present work is that the fluid bulk temperature reaches a value higher than the constant wall temperature, even when the fluid at the inlet is cooler than the wall, as shown in Fig. 5. This value is constant at a given set of Pe, Br and Kn, which represent the viscous dissipation, axial condition and rarified effects.

To detailedly illustrate this convergence development of the fluid bulk temperature at various inlet conditions, we test the developments of T_b at various viscous conditions represented by $|Br|$, as shown in Fig. 6. The rarified effect and axial conduction are excluded by setting $Kn = 0$ and $Pe = 10^6$, as will be explained later in the following sections. $Br > 0$ and $Br < 0$ correspond to the cases where the fluid inlet temperature is higher and lower than the constant wall temperature, respectively, as defined in Eq. (3). For both cases, the asymptotic dimensionless fluid temperature converges to the same value θ_{bF} ($\theta_{bF} = \frac{T_{bF}-T_w}{T_i-T_w}$). This result is robust even when the initial conditions (ΔT and $\Delta T'$ in Fig. 6) are varied. A similar temperature overshoot without an exact value was reported before in separated cooling and heating tests [38, 39]. In the present study, it is clarified that, because viscous dissipation generates an additional amount of heat, the asymptotic temperature of the fluid is always higher than the constant wall temperature, regardless of the inlet condition of the fluid. Further, the exact temperature overshoot and its dependence on Pe, Br and Kn are obtained. In addition, care must be taken that there is a critical point denoted as ξ_c in Fig. 6 as reported in literatures [17, 24, 25]. The fluid bulk temperature is equal to the wall temperature at this point for $Br < 0$ cases. Clearly, ξ_c can be interpreted as the effective length of the channel for cooling. It is also seen in the figure that a higher temperature overshoot corresponds to a lower length of the channel for effective cooling.

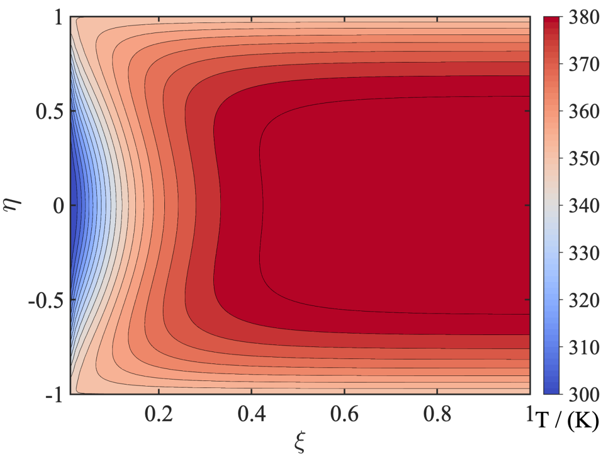

Figure 5: The contour of temperature in the 2D channel at $Pe = 10^6, Kn = 0.00, Br = -1.0$ (The inlet temperature of the fluid and the wall temperature are 300 K and 350 K, respectively).

Then we turn to the development of the fluid non-dimensional bulk temperature at more general conditions. Fig. 7 shows the profile of the bulk temperature at various viscous and rarified conditions, while the axial conduction is still neglected by setting $Pe = 10^6$. At $Br = 0$, where there is no viscous dissipation, $\theta_{bF} = 0$ for all the cases considered. With increasing Br, θ_{bF} increases almost linearly for all Kn considered. Also, θ_{bF} roughly reduces at higher Kn. Here Kn quantifies the rarified effects as will be shown later and as it increases, the fluid flow moves from the continuous flow regime ($Kn = 0$ corresponds to the continuum flow regime as

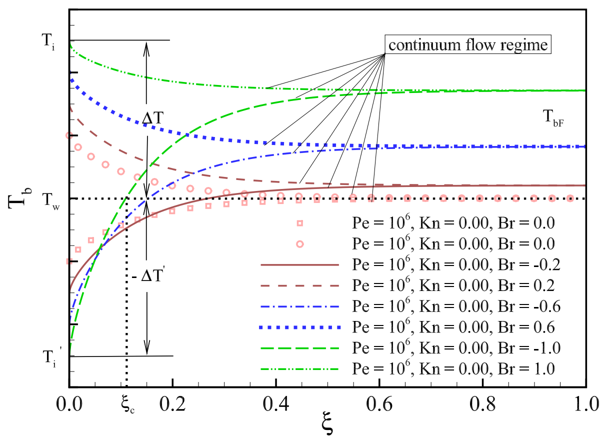

Figure 6: Fluid dimensionless bulk temperature profile.

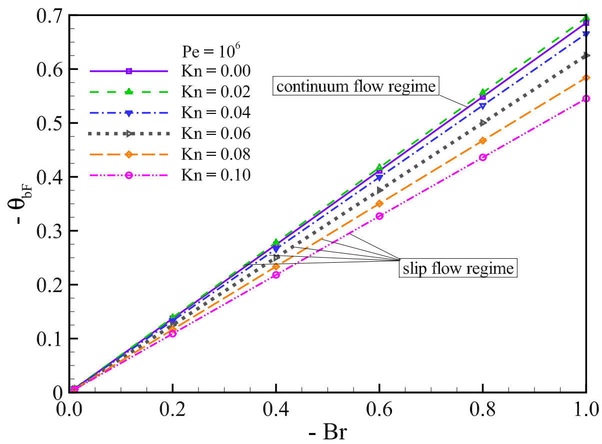

Figure 7: Fluid asymptotic dimensionless bulk temperature profile when neglecting axial conduction.

reported by [40]) to the slip-flow regime (see Fig. 7). Similar results (not shown here) have been observed for $Pe = 10$, where the axial conduction effect is activated.

These observations indicate that the magnitude of the overshooting fluid dimensionless bulk temperature is a linear function of Br, and it vanishes when the viscous dissipation is neglected. This overshoot reduces with Kn, the rarified effect, but is insensitive to Pe, the axial conduction effect.

The critical point ξ_c observed in Fig. 6, at which the temperature of fluids is equal to the wall temperature, deserves further studies and the variation of ξ_c with respect to Br, Pe and Kn is investigated. In Fig. 8a, 36 cases (considering six values of Kn and six values of Br at each Kn) are studied to reveal effects of Kn and Br on ξ_c when neglecting axial conduction by setting $Pe = 10^6$, and then 45 cases including five values of Kn

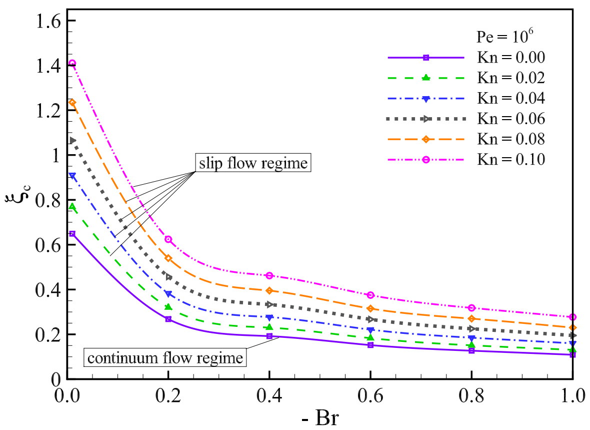

(a)

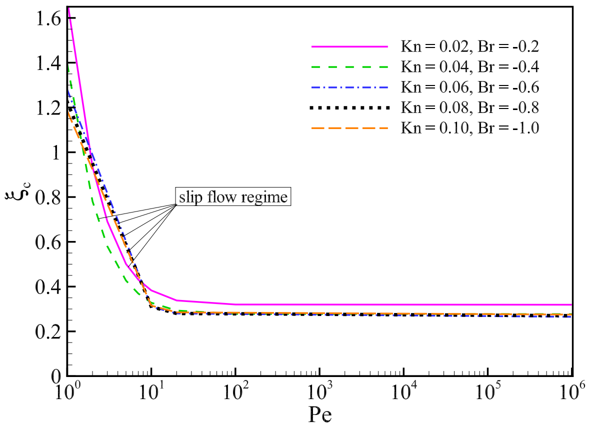

(b)

Figure 8: Distribution of the critical length ξ_c. (a) ξ_c changes with Br and Kn when neglecting axial conduction. (b) ξ_c profile at different Pe.

and Br (nine values of Pe at each group of Kn and Br) are conducted to further examine how Pe affects ξ_c in Fig. 8b. Clearly, ξ_c reduces with larger Br and Pe and smaller Kn, corresponding to stronger viscous dissipation, weaker axial conduction and weaker rarified effect, respectively.

5. Parameter dependence of the heat transfer

It has been shown that three parameters Kn, Pe and Br have critical roles in the temperature overshoot. Each of them will be studied individually in this section to illustrate their effects on the heat transfer between the fluid and the channel, quantified by the local and asymptotic Nusselt number, dimensionless temperature jump and non-dimensional bulk temperature profiles.

5.1. *Effect of viscous dissipation*

The effect of Br on Nu_L when neglecting the rarefied effect and axial conduction is illustrated in Fig. 9. Based on Eq. (3), $Br > 0$ and $Br < 0$ mean that the inlet temperature of the fluid is higher or lower than the uniform wall temperature, respectively. $Br = 0$ indicates that the viscous dissipation is not taken into consideration. It can be seen from the figure that if neglecting Kn and Pe effects the asymptotic Nusselt number with or without viscous dissipation is 17.5 or 7.54 (the latter value is in agreement with previous studies [26, 41], which further validates the present analytical solution approach of the 2D energy equation), respectively. Clearly, these values suggest that $Br = 0$ is a singular point where the change of Nusselt number is discontinuous. This singularity can be validated analytically. After substituting Eq. (7) and Eq. (24) into Eq. (25), Nu_L can be written as

$$Nu_L = \frac{-4\left[\left.\frac{\partial\theta_1(\eta)}{\partial\eta}\right|_{\eta=1} + \left.\frac{\partial\theta_2(\xi,\eta)}{\partial\eta}\right|_{\eta=1}\right]}{\int_0^1 u^*(\eta)\left[\theta_1(\eta)+\theta_2(\xi,\eta)\right]\,d\eta}, \tag{27}$$

where θ_1 and θ_2 are shown in Eq. (13) and Eq. (22), respectively. For all cases mentioned in this sub-section, Nu_L is

$$Nu_L = \frac{-4\left[-3Br + \left.\frac{\partial\theta_2(\xi,\eta)}{\partial\eta}\right|_{\eta=1}\right]}{\frac{24}{35}Br + \int_0^1 u^*(\eta)\,\theta_2(\xi,\eta)\,d\eta}. \tag{28}$$

When $Br \neq 0$ and $\xi \to +\infty$, $\theta_2(\xi,\eta)$ tends to 0. Hence, the asymptotic Nusselt number is

$$Nu_F = \frac{12Br}{\frac{24}{35}Br} = 17.5. \tag{29}$$

Obviously, if $Br = 0$, we have

$$Nu_F = \lim_{\xi\to+\infty}\left[\frac{-4\left.\frac{\partial\theta_2(\xi,\eta)}{\partial\eta}\right|_{\eta=1}}{\int_0^1 u^*(\eta)\,\theta_2(\xi,\eta)\,d\eta}\right] = 7.54. \tag{30}$$

Moreover, it is worth noting that $Br < 0$ induces a singular point where Nu_L approximates infinity. This is caused by the definition of the Nusselt number ($Nu_L = -\frac{4}{\theta_b(\xi)}\left.\frac{\partial\theta(\xi,\eta)}{\partial\eta}\right|_{\eta=1}$). There is a point where the dimensionless bulk temperature of fluid is equal to wall temperature (so θ_b is equal to 0.) as can be found in Fig. 10.

The bulk dimensionless temperature profiles at various Br number without Pe and Kn effect are described in Fig. 10. The difference between asymptotic fluid

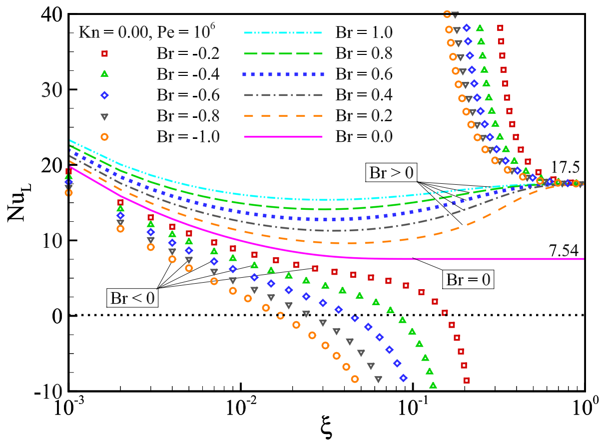

Figure 9: Viscous dissipation effect on local Nusselt number

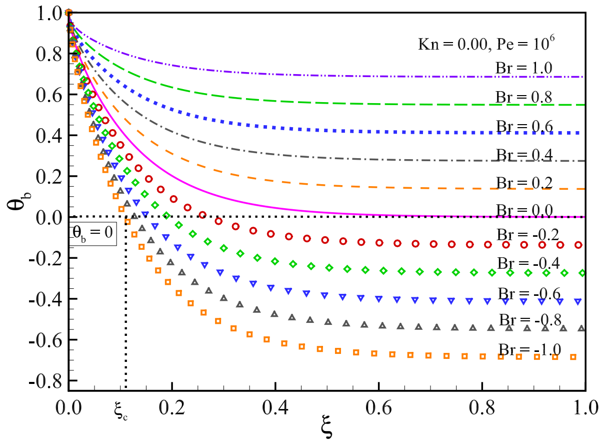

Figure 10: Viscous dissipation effect on bulk dimensionless temperature

bulk temperature and inlet temperature of fluid increases with a reduction in Br if $Br > 0$. The asymptotic fluid temperature equals to wall temperature for $Br = 0$ corresponding to neglecting viscous dissipation. As mentioned in Section 4 for $Br < 0$ cases, it can be still observed that there is a critical point ξ_c. θ_b equal to 0 at this point, which means the fluid temperature equal to the wall temperature. For $\xi > \xi_c$, θ_b will be less than 0, suggesting that the fluid temperature exceeds the wall temperature, and the effective cooling length is reduced with an increase in $|Br|$. These observations indicate that the cooling effect will be over-estimated when neglecting viscous dissipation.

5.2. *Effect of axial conduction*

It is well known that axial conduction can rise in instances of small Re and Pr since thermal diffusion becomes more important than advection. The dimensionless Pe is usually applied to characterize the effect of axial conduction. As discussed in the introduction, there has been no consensus on the impact of axial conduction on heat transfer. Hence, nine cases ($Pe = 1, Pe = 2, Pe = 3, Pe = 5, Pe = 7, Pe = 10, Pe = 20, Pe = 100, Pe = 10^6$) are performed to clarify its influence.

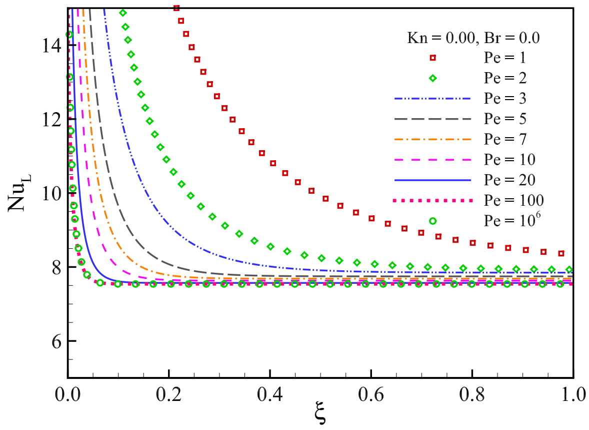

(a)

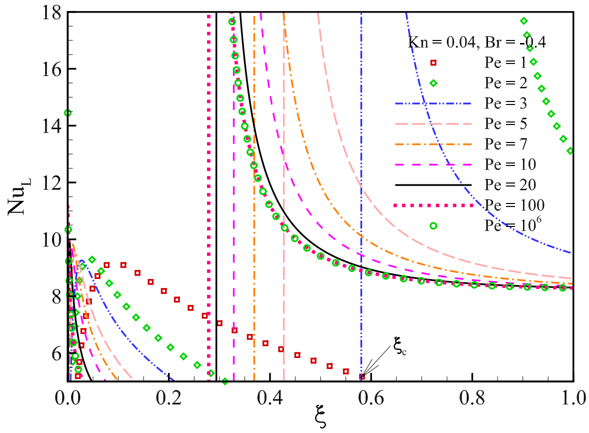

(b)

Figure 11: Local Nusselt number at various Pe number when considering rarefied effects and viscous dissipation (a) or not (b).

As shown in Fig. 11a, local Nusselt numbers for nine cases converge to various asymptotic values when neglecting the rarefied effect and viscous dissipation. However, for $Pe = 1$ or below, Nu is much larger than other cases especially in the thermal developing region. δ_{Nu} (defined as the relative difference of Nu_L , $\delta_{Nu} = \frac{Nu_L - Nu_L|_{Pe=10^6}}{Nu_L|_{Pe=10^6}} \times 100\%$) decreases rapidly and then maintains a constant level along the flow direction. The value of δ_{Nu} is below 10% for $Pe = 20$,

$Pe = 10$, $Pe = 7$, $Pe = 5$, $Pe = 3$ and $Pe = 2$ at axial non-dimensional coordinate $\xi \geqslant 0.039$, $\xi \geqslant 0.081$, $\xi \geqslant 0.118$, $\xi \geqslant 0.17$, $\xi \geqslant 0.301$, $\xi \geqslant 0.478$, respectively. δ_{Nu} for $Pe = 100$ is always less than 7%, while δ_{Nu} for $Pe = 1$ is greater than 10% along the flow direction. This indicates that: (1) the axial conduction effect on asymptotic Nusselt number Nu_F can be neglected if $Pe > 10$. (2) its influence on local and asymptotic Nusselt number is negligible when $Pe > 100$. (3) if $Pe < 1$, the axial conduction must be considered.

The variation of Nu_L is examined at various values of Pe with $Kn = 0.04$ and $Br = -0.4$ to take the rarefied effect and viscous dissipation into consideration in Fig. 11b. When $\xi \geqslant 0.512$ (or $\xi \geqslant 0.375$), δ_{Nu} at $Pe = 10$ (or $Pe = 20$) is less than 10%. Also, δ_{Nu} at $Pe = 1$ is always high than 50% and δ_{Nu} at $Pe = 100$ is below 5%. Hence, similar conclusions about the axial conduction effect can be drawn when considering the rarefied effect and viscous dissipation. The consideration of Kn and Br effects induces a singular point at which Nu_L approaches infinity because the denominator θ_b vanishes (see Eq. (25)) at the critical point ξ_c as can be seen from Fig. 12b. Moreover, ξ_c gradually moves toward the inlet of the channel at larger Pe, which is in agreement with Fig. 8b.

Then the effects of axial conduction on the bulk non-dimensional temperature θ_b are examined, as shown in Fig. 12a. Here the rarefied effect and viscous dissipation are not considered by setting $Kn = 0$ and $Br = 0$. It is seen from the figure that, the rate of bulk temperature variation for $Pe = 1$ is obviously much slower than the other cases, as convection plays a more important role than conduction for extremely small Pe number. The relative difference of bulk temperature profile δ_θ ($\delta_\theta = \frac{\theta_b - \theta_b|_{Pe=10^6}}{\theta_b|_{Pe=10^6}}$) for $Pe = 100$ is less than 0.04 in all the fluid flow direction although $\theta_b|_{Pe=10^6}$ may cause other mathematical difference as this value tends to be 0 at the end of the channel. The effects of axial conduction on bulk dimensionless temperature, therefore, are negligible in the range $Pe > 100$. When the Kn effect and Br effect are accounted, as shown in Fig. 12b, similar results on the axial conduction can be observed.

5.3. Rarefied effect

The effect of Kn number characterizing rarefaction on the local Nusselt number is examined, as described in Fig. 13. $Pe = 10^6$ and $Br = 0$ are adopted, leading to negligible axial conduction and viscous dissipation. Along the ξ axis, the Nusselt number only varies around the entrance and then reaches a constant value. The asymptotic Nusselt number Nu_F is 7.54 at $Kn = 0$

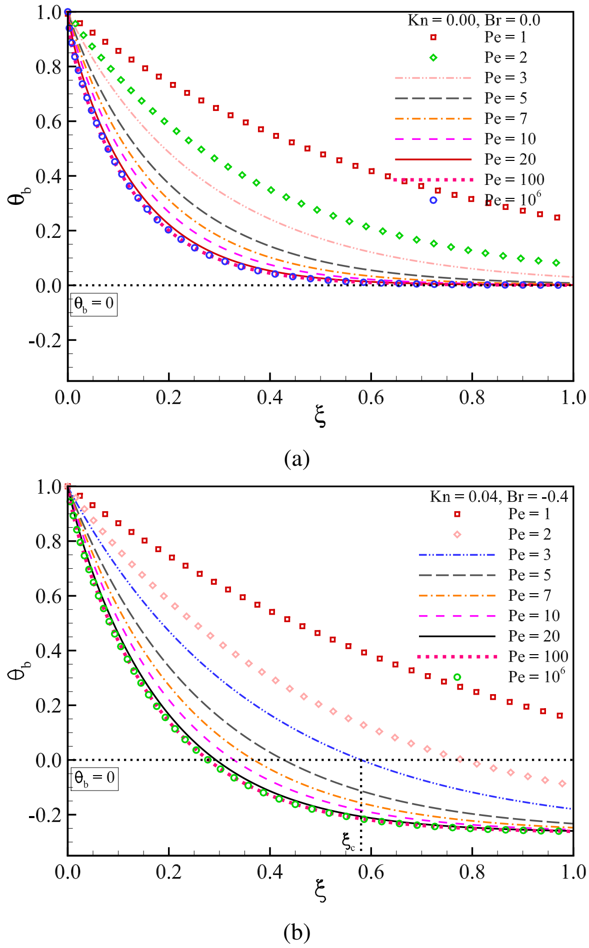

Figure 12: Bulk dimensionless temperature profile when neglecting rarefied effects and viscous dissipation (a) or not (b).

as reported in Section 5.1. Also, Nu_F decreases nonlinearly with the increasing of Kn.

As shown in Fig. 14, unlike the Nusselt number which approaches quickly to an asymptotic value in the axial direction, the fluid temperature jump occurs over the entire channel and becomes more obvious at higher Kn number. In addition, the temperature jump θ_s is 0 for $Pe = 10^6, Br = 0.00, Kn = 0.00$, and it can be also seen obviously that the fluid temperature near the wall is equal to zero from Eq. (5c) for the same case. This indicates that the truncation of the infinite series in Section 2 does not cause a significant difference in the analytical solution of the dimensionless energy equation and further validates the present method.

Fig. 15 is for the non-dimensional fluid bulk temperature distribution along the flow direction without axial conduction and viscous dissipation. Similarly with θ_s, the bulk temperature also varies across the whole

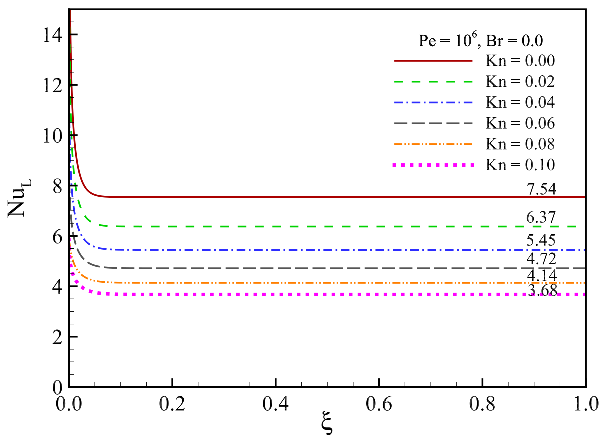

Figure 13: Rarefied effect on local Nusselt number

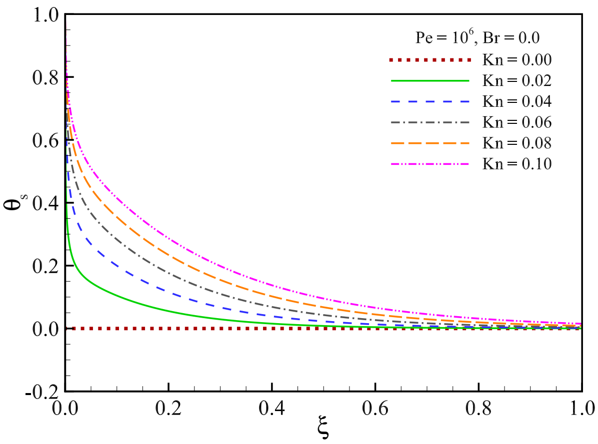

Figure 14: Rarefied effect on dimensionless temperature jump at the wall

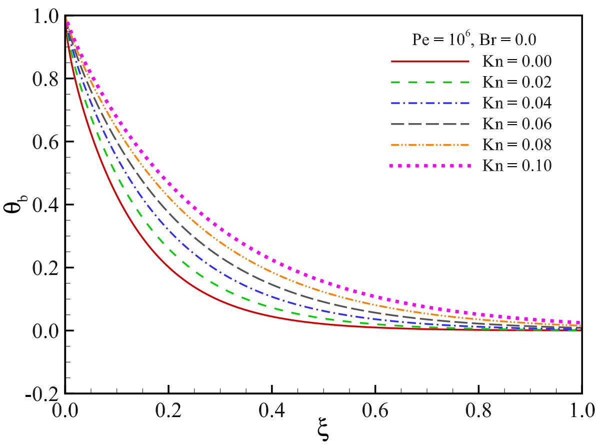

Figure 15: Rarefied effect on bulk dimensionless temperature

channel. At $Kn = 0$, the bulk temperature keeps a constant value in the second half of the channel. This indicates that, in this continuous regime, heat transfer between the fluid and the solid materials only occurs around the first half of the channel. As Kn increases, however, the bulk temperature variation along the axis becomes more mild, revealing the potential to deliver cooling effect along the whole channel. This will be particularly useful when cooling a hot surface through micro or nanochannels.

6. Conclusions

We apply the separation of variables method and the variable substitution approach to obtain an infinite series solution of the 2D energy equation with a first-order velocity slip model and a first-order temperature jump model. In this novel approach, firstly, the energy equation is represented by the sum of two sub-functions via the separation of variables method. One subfunction can be solved immediately, and the other one can be written as the infinite series form whose terms consist of an exponential function, an unknown function and an underdetermined coefficient. The undetermined function can be represented by the product of the Kummer's confluent hypergeometric function and another exponential function through the variable substitution approach. Then, the unknown coefficient is determined via applying the Gram-Schmidt orthogonalization accompanied with Gauss-Legendre quadrature. Finally, the analytic solution of the energy equation is obtained, and applied to study effects of the viscous dissipation, axial conduction and rarefaction on heat transfer. The following conclusions can be drawn from this study:

- The asymptotic non-dimensional bulk temperature of fluid $|\theta_{bF}|$ converges to a constant value higher than the wall temperature regardless of the inlet condition at a given set of Pe, Br ($Br \neq 0$) and Kn. This value increases linearly with Br, drops slightly at higher Kn, and is almost independent on Pe.
- If a fluid is used to cool the wall with uniform temperature, there is a critical point where the fluid bulk temperature reaches the same value as wall temperature and the Nusselt number becomes ill-defined at this point. This point moves much closer to the channel entrance at increasing $|Br|$ or Pe. On the contrary, the point moves towards the end of the channel with increasing Kn.
- By eliminating the rarefied effect and axial conduction, the asymptotic Nusselt number with or without viscous dissipation is 17.5 or 7.54, respectively.

- The axial conduction effect on asymptotic Nusselt number can be neglected if $Pe > 10$ while the effect of axial conduction on the local Nusselt number and bulk non-dimensional temperature are negligible when $Pe > 100$.
- The rarified effect on the local Nusselt number is localized around the entrance of the channel, but is across the whole channel for the bulk temperature and temperature jump. At a larger Kn, the bulk temperature variation along the axis becomes milder, revealing the potential to deliver cooling effect along the whole channel.

7. Acknowledgements

We would like to acknowledge financial support under the Engineering and Physical Sciences Research Council grant EP/M025039/2 and China Scholarship Council (CSC).

Appendix A. Gram-Schmidt orthogonal approach

Let us assume a series of orthogonal function g_i to make

$$\theta_2 = \sum A_n f_n exp(-\beta_n^2 \xi) = \sum B_n g_n exp(-\beta_n^2 \xi), \quad \text{(A.1)}$$

where B_n is also the summation coefficient. The relation between g_i and eigenfunction is

$$g_1 = f_1 \quad \text{(A.2a)}$$
$$g_2 = f_2 - \alpha_{21} f_1 \quad \text{(A.2b)}$$
$$g_3 = f_3 - \alpha_{31} f_1 - \alpha_{32} f_2 \quad \text{(A.2c)}$$
$$g_4 = f_4 - \alpha_{41} f_1 - \alpha_{42} f_2 - \alpha_{43} f_3 \quad \text{(A.2d)}$$
$$\vdots$$
$$g_N = f_N - \sum_{j=1,N>=2}^{N-1} \alpha_{Nj} f_j, \quad \text{(A.2e)}$$

where α_{ij} are constants. In the following step, efforts are made to calculate these constants before determining orthogonal functions g_i. For convenience, we apply a symbol $\otimes$ and define

$$\int_0^1 f \cdot g \, d\eta = f \otimes g. \quad \text{(A.3)}$$

Now by multiplying Eq. (A.2b) with g_1 and integrating over the domain $(0 \leqslant \eta \leqslant 1)$ based on the property of orthogonal function, we can obtain

$$g_2 \otimes g_1 = f_2 \otimes g_1 - \alpha_{21} f_1 \otimes g_1 = 0, \quad \text{(A.4)}$$

and then α_{21} is

$$\alpha_{21} = \frac{f_2 \otimes g_1}{f_1 \otimes g_1}. \quad \text{(A.5)}$$

Then we respectively multiply Eq. (A.2c) with g_1, g_2 and perform integration in domain $(0 \leqslant \eta \leqslant 1)$

$$g_3 \otimes g_1 = f_3 \otimes g_1 - \alpha_{31} f_1 \otimes g_1 - \alpha_{32} f_2 \otimes g_1 = 0 \quad \text{(A.6a)}$$
$$g_3 \otimes g_2 = f_3 \otimes g_2 - \alpha_{31} f_1 \otimes g_2 - \alpha_{32} f_2 \otimes g_2 = 0 \quad \text{(A.6b)}$$

The above Eqs. (A.6a) and (A.6b) can be written as a matrix

$$\begin{bmatrix} f_1 \otimes g_1 & f_2 \otimes g_1 \\ f_1 \otimes g_2 & f_2 \otimes g_2 \end{bmatrix} \begin{bmatrix} \alpha_{31} \\ \alpha_{32} \end{bmatrix} = \begin{bmatrix} f_3 \otimes g_1 \\ f_3 \otimes g_2 \end{bmatrix}. \quad \text{(A.7)}$$

Similarly, we can also multiply respectively Eq. (A.2d) with g_1, g_2 and g_3, and Eq. (A.2e) with g_1, g_2, $\cdots$ g_{N-1}, integrate all terms in these equations over the zone $(0 \leqslant \eta \leqslant 1)$ and rearrange these into matrix form

$$\begin{bmatrix} f_1 \otimes g_1 & f_2 \otimes g_1 & f_3 \otimes g_1 \\ f_1 \otimes g_2 & f_2 \otimes g_2 & f_3 \otimes g_2 \\ f_1 \otimes g_3 & f_2 \otimes g_3 & f_3 \otimes g_3 \end{bmatrix} \begin{bmatrix} \alpha_{41} \\ \alpha_{42} \\ \alpha_{43} \end{bmatrix} = \begin{bmatrix} f_4 \otimes g_1 \\ f_4 \otimes g_2 \\ f_4 \otimes g_3 \end{bmatrix} \quad \text{(A.8a)}$$

$$\vdots$$

$$\begin{bmatrix} f_1 \otimes g_1 & f_2 \otimes g_1 & \cdots & f_{N-1} \otimes g_1 \\ f_1 \otimes g_2 & f_2 \otimes g_2 & \cdots & f_{N-1} \otimes g_2 \\ \vdots & \vdots & \vdots & \vdots \\ f_1 \otimes g_{N-1} & f_2 \otimes g_{N-1} & \cdots & f_{N-1} \otimes g_{N-1} \end{bmatrix} \begin{bmatrix} \alpha_{N1} \\ \alpha_{N2} \\ \vdots \\ \alpha_{NN-1} \end{bmatrix} = \begin{bmatrix} f_N \otimes g_1 \\ f_N \otimes g_2 \\ \vdots \\ f_N \otimes g_{N-1} \end{bmatrix}. \quad \text{(A.8b)}$$

In addition to that, according to Eqs. (A.2a) to (A.2e) and property of orthogonal function, we can get

$$f_m \otimes g_n = 0, \qquad if \qquad (m < n). \quad \text{(A.9)}$$

Hence, Eq. (A.7) and Eqs. (A.8a) and (A.8b) could be simplified to

$$\begin{bmatrix} f_1 \otimes g_1 & f_2 \otimes g_1 \\ 0 & f_2 \otimes g_2 \end{bmatrix} \begin{bmatrix} \alpha_{31} \\ \alpha_{32} \end{bmatrix} = \begin{bmatrix} f_3 \otimes g_1 \\ f_3 \otimes g_2 \end{bmatrix}, \tag{A.10a}$$

$$\begin{bmatrix} f_1 \otimes g_1 & f_2 \otimes g_1 & f_3 \otimes g_1 \\ 0 & f_2 \otimes g_2 & f_3 \otimes g_2 \\ 0 & 0 & f_3 \otimes g_3 \end{bmatrix} \begin{bmatrix} \alpha_{41} \\ \alpha_{42} \\ \alpha_{43} \end{bmatrix} = \begin{bmatrix} f_4 \otimes g_1 \\ f_4 \otimes g_2 \\ f_4 \otimes g_3 \end{bmatrix} \tag{A.10b}$$

$$\begin{bmatrix} f_1 \otimes g_1 & f_2 \otimes g_1 & \cdots & f_{N-1} \otimes g_1 \\ 0 & f_2 \otimes g_2 & \cdots & f_{N-1} \otimes g_2 \\ \vdots & \vdots & \vdots & \vdots \\ 0 & 0 & \cdots & f_{N-1} \otimes g_{N-1} \end{bmatrix} \cdot \begin{bmatrix} \alpha_{N1} \\ \alpha_{N2} \\ \vdots \\ \alpha_{NN-1} \end{bmatrix} = \begin{bmatrix} f_N \otimes g_1 \\ f_N \otimes g_2 \\ \vdots \\ f_N \otimes g_{N-1} \end{bmatrix}. \tag{A.10c}$$

These above equations can be simply written as a matrix equation

$$\boldsymbol{L} \cdot \boldsymbol{V} = \boldsymbol{R}. \tag{A.11}$$

From Eqs. (A.2a) to (A.2e) and (A.10a) to (A.10c), all coefficients α_{nm} and orthogonal functions g_i could be obtained. In the following section, we will make effort to determine coefficients B_n from initial boundary condition $\xi = 0, \theta = 1$. Based on $\theta = \theta_1 + \theta_2$ and the boundary condition, we can get

$$\begin{aligned} &\theta = \theta_1 + \theta_2 = \theta_1 + \sum A_n f_n exp(-\beta_n^2 \xi) \\ &= \theta_1 + \sum B_n g_n exp(-\beta_n^2 \xi) = 1. \end{aligned} \tag{A.12}$$

Multiply Eq. (A.12) with g_n and conducting integration in zone $[0, 1]$ and then coefficients B_n may be calculated from

$$B_n = \frac{(1 - \theta_1) \otimes g_n}{g_n \otimes g_n}. \tag{A.13}$$

When $\xi = 0$, the Eq. (A.1) is transformed into

$$\sum A_n f_n = \sum B_n g_n. \tag{A.14}$$

Then, Eqs. (A.2a) to (A.2e) are substituted in Eq. (A.14)

$$\begin{aligned} &\sum A_n f_n = \sum B_n g_n \\ &= B_1 g_1 + B_2 g_2 + B_3 g_3 + B_4 g_4 + \cdots + B_N g_N \\ &= B_1 f_1 + B_2 (f_2 - \alpha_{21} f_1) + B_3 (f_3 - \alpha_{31} f_1 - \alpha_{32} f_2) \\ &+ B_4 (f_4 - \alpha_{41} f_1 - \alpha_{42} f_2 - \alpha_{43} f_3) \\ &+ \cdots \\ &+ B_N \left(f_N - \sum_{j=1, N>=2}^{N-1} \alpha_{Nj} f_j \right) \\ &= (B_1 - \alpha_{21} B_2 - \alpha_{31} B_3 - \alpha_{41} B_4 - \cdots - \alpha_{N1} B_N) f_1 \\ &+ (B_2 - \alpha_{32} B_3 - \alpha_{42} B_4 - \cdots - \alpha_{N2} B_N) f_2 \\ &+ (B_3 - \alpha_{43} B_4 - \cdots - \alpha_{N3} B_N) f_3 \\ &+ (B_4 - \cdots - \alpha_{N4} B_N) f_4 \\ &+ \cdots \\ &+ B_N f_N. \end{aligned} \tag{A.15}$$

Hence, coefficients A_n become

$$\begin{aligned} &A_1 = B_1 - \alpha_{21} B_2 - \alpha_{31} B_3 - \alpha_{41} B_4 - \cdots - \alpha_{N1} B_N \\ &A_2 = B_2 - \alpha_{32} B_3 - \alpha_{42} B_4 - \cdots - \alpha_{N2} B_N \\ &A_3 = B_3 - \alpha_{43} B_4 - \cdots - \alpha_{N3} B_N \\ &A_4 = B_4 - \cdots - \alpha_{N4} B_N \\ &\quad \ldots \\ &A_N = B_N. \end{aligned} \tag{A.16}$$

That is

$$\begin{aligned} &A_n = B_n - \sum_{m=n+1}^{N} \alpha_{mn} B_m \quad at \quad 1 \leqslant n \leqslant N - 1 \\ &A_N = B_N. \end{aligned} \tag{A.17}$$

Appendix B. The algorithm about applying the Gram-Schmidt orthogonal approach to determine summation constants

Start of the algorithm determining coefficients A_n by applying Gram-Schmidt orthogonal procedure.

Step 1. Determine eigenvalues β_n $(1 \leqslant n \leqslant N)$ from the boundary condition in Eq. (16b). N is the number of eigenvalues or eigenfunctions.

Step 2. Define a user function that can integrate the product of two arbitrary functions over the arbitrary domain $[a, b] (a < b)$ by using the Gauss-Legendre quadrature method as this method can calculate numerical integration with high accuracy and short CPU times.

Step 3. Input β_n, Pe, a_n, b_n, N to obtain $f_n(\eta)$.

Step 4. Calculate g_1 on the basis of Eq. (A.2a), α_{21} from on the basis of Eq. (A.5)and g_2 based on Eq. (A.2b) respectively. Store g_1 and g_2 into a list named g.

Step 5. Set an index number p=3.

Step 6. Apply the user definition integration function in Step 2 to determine the left matrix $\boldsymbol{L}$, the right matrix $\boldsymbol{R}$ and vector $\boldsymbol{V}$ in Eq. (A.11) and g_p. Store g_p in a list g and set $p = p + 1$.

Step 7. Compare the p and N
if ($p \leqslant N$)
    go to Step 6.
else
    move to the next step.

Step 8. Calculate coefficients B_n based on boundary condition.

Step 9. Determine coefficients A_n from Eq. (A.17).

End of the algorithm.

Appendix C. First 20 eigenvalues and coefficients

Two tables given below show the first 20 eigenvalues and summation coefficients determined via using the Gram-Schmidt orthogonal approach at various Knudsen number and Brinkman number.

Table C.1: First 20 eigenvalues and coefficients for $Pe = 10^6, Br = 0.00$

n	Kn=0.00		Kn=0.04		Kn=0.08	
	β_n	A_n	β_n	A_n	β_n	A_n
1	2.7460	1.2010	2.3336	1.1768	2.0341	1.1481
2	9.2588	-0.2997	8.1700	-0.2517	7.5513	-0.2007
3	15.7882	0.1616	14.1779	0.1160	13.4858	0.0781
4	22.3192	-0.1085	20.2895	-0.0667	19.6004	-0.0401
5	28.8507	0.0810	26.4707	0.0431	25.7994	0.0241
6	35.3824	-0.0644	32.6992	-0.0299	32.0425	-0.0159
7	41.9142	0.0535	38.9603	0.0219	38.3110	0.0113
8	48.4460	-0.0458	45.2446	-0.0167	44.5954	-0.0084
9	54.9779	0.0401	51.5457	0.0131	50.8901	0.0065
10	61.5098	-0.0359	57.8592	-0.0106	57.1921	-0.0052
11	68.0417	0.0326	64.1822	0.0087	63.4994	0.0042
12	74.5737	-0.0301	70.5125	-0.0073	69.8104	-0.0035
13	81.1056	0.0282	76.8486	0.0062	76.1244	0.0030
14	87.6376	-0.0268	83.1893	-0.0054	82.4407	-0.0025
15	94.1695	0.0258	89.5338	0.0047	88.7588	0.0022
16	100.7015	-0.0253	95.8814	-0.0042	95.0784	-0.0019
17	107.2334	0.0254	102.2315	0.0038	101.3991	0.0017
18	113.7654	-0.0263	108.5839	-0.0035	107.7208	-0.0016
19	120.2973	0.0290	114.9380	0.0034	114.0434	0.0015
20	126.8293	-0.0380	121.2937	-0.0037	120.3667	-0.0015

Table C.2: First 20 eigenvalues and coefficients for $Pe = 10^6, Kn = 0.00$

n	Br=0.0		Br=0.2		Br=-0.2	
	β_n	A_n	β_n	A_n	β_n	A_n
1	2.7460	1.2010	2.7460	1.0285	2.7460	1.3735
2	9.2588	-0.2997	9.2588	-0.2710	9.2588	-0.3283
3	15.7882	0.1616	15.7882	0.1529	15.7882	0.1704
4	22.3192	-0.1085	22.3192	-0.1046	22.3192	-0.1124
5	28.8507	0.0810	28.8507	0.0789	28.8507	0.0832
6	35.3824	-0.0644	35.3824	-0.0631	35.3824	-0.0658
7	41.9142	0.0535	41.9142	0.0526	41.9142	0.0544
8	48.4460	-0.0458	48.4460	-0.0452	48.4460	-0.0464
9	54.9779	0.0401	54.9779	0.0397	54.9779	0.0406
10	61.5098	-0.0359	61.5098	-0.0355	61.5098	-0.0362
11	68.0417	0.0326	68.0417	0.0324	68.0417	0.0329
12	74.5737	-0.0301	74.5737	-0.0299	74.5737	-0.0303
13	81.1056	0.0282	81.1056	0.0280	81.1056	0.0284
14	87.6376	-0.0268	87.6376	-0.0266	87.6376	-0.0269
15	94.1695	0.0258	94.1695	0.0257	94.1695	0.0259
16	100.7015	-0.0253	100.7015	-0.0252	100.7015	-0.0254
17	107.2334	0.0254	107.2334	0.0253	107.2334	0.0255
18	113.7654	-0.0263	113.7654	-0.0262	113.7654	-0.0264
19	120.2973	0.0290	120.2973	0.0289	120.2973	0.0291
20	126.8293	-0.0380	126.8293	-0.0378	126.8293	-0.0381

[1] C.-M. Ho, Y.-C. Tai, Micro-electro-mechanical-systems (mems) and fluid flows, Annual Review of Fluid Mechanics 30 (1) (1998) 579–612.

[2] M. Gad-el Hak, The fluid mechanics of microdevices—the freeman scholar lecture, Journal of Fluids Engineering 121 (1) (1999) 5–33.

[3] G. Cerri, A. Giovannelli, L. Battisti, R. Fedrizzi, Advances in effusive cooling techniques of gas turbines, Applied Thermal Engineering 27 (4) (2007) 692–698.

[4] J. Zhao, J. Yao, M. Zhang, L. Zhang, Y. Yang, H. Sun, S. An, A. Li, Study of gas flow characteristics in tight porous media with a microscale lattice boltzmann model, Scientific reports 6 (2016) 32393.

[5] S. Choi, Fluid flow and heat transfer in microtubes, Micromechanical Sensors, Actuators, and Systems, ASME (1991) 123–134.

[6] J. C. Harley, Y. Huang, H. H. Bau, J. N. Zemel, Gas flow in micro-channels, Journal of Fluid Mechanics 284 (1995) 257–274.

[7] C. Tso, S. Mahulikar, The use of the brinkman number for single phase forced convective heat transfer in microchannels, International Journal of Heat and Mass Transfer 41 (12) (1998) 1759–1769.

[8] C. Tso, S. Mahulikar, The role of the brinkman number in analysing flow transitions in microchannels, International Journal of Heat and Mass Transfer 42 (10) (1999) 1813–1833.

[9] C. Tso, S. Mahulikar, Experimental verification of the role of brinkman number in microchannels using local parameters, International Journal of Heat and Mass Transfer 43 (10) (2000) 1837–1849.

[10] G. Tunc, Y. Bayazitoglu, Heat transfer in microtubes with viscous dissipation, International Journal of Heat and Mass Transfer 44 (13) (2001) 2395–2403.

[11] G. Tunc, Y. Bayazitoglu, Heat transfer in rectangular microchannels, International Journal of Heat and Mass Transfer 45 (4) (2002) 765–773.

[12] J. Koo, C. Kleinstreuer, Viscous dissipation effects in microtubes and microchannels, International Journal of Heat and Mass Transfer 47 (14-16) (2004) 3159–3169.

[13] M. Michelsen, J. Villadsen, The graetz problem with axial heat conduction, International Journal of Heat and Mass Transfer 17 (11) (1974) 1391–1402.

[14] J. Lahjomri, A. Oubarra, Analytical solution of the graetz problem with axial conduction, Journal of heat transfer 121 (4) (1999) 1078–1083.

[15] J. Lahjomri, A. Oubarra, A. Alemany, Heat transfer by laminar hartmann flow in thermal entrance region with a step change in wall temperatures: the graetz problem extended, International journal of heat and mass Transfer 45 (5) (2002) 1127–1148.

[16] B. Weigand, D. Lauffer, The extended graetz problem with

piecewise constant wall temperature for pipe and channel flows, International journal of heat and mass transfer 47 (24) (2004) 5303–5312.

[17] I. Tiselj, G. Hetsroni, B. Mavko, A. Mosyak, E. Pogrebnyak, Z. Segal, Effect of axial conduction on the heat transfer in micro-channels, International Journal of Heat and Mass Transfer 47 (12-13) (2004) 2551–2565.

[18] G. Maranzana, I. Perry, D. Maillet, Mini-and micro-channels: influence of axial conduction in the walls, International journal of heat and mass transfer 47 (17-18) (2004) 3993–4004.

[19] W. Minkowycz, A. Haji-Sheikh, Heat transfer in parallel plates and circular porous passages with axial conduction, International journal of heat and mass transfer 49 (13-14) (2006) 2381–2390.

[20] A. Haji-Sheikh, J. Beck, D. E. Amos, Axial heat conduction effects in the entrance region of circular ducts, Heat and Mass Transfer 45 (3) (2009) 331–341.

[21] Y.-W. Gu, S. Ge, M. Chen, A molecular dynamics simulation of nanoscale convective heat transfer with the effect of axial heat conduction, Molecular Physics 114 (12) (2016) 1922–1930.

[22] D. Hennecke, Heat transfer by hagen-poiseuille flow in the thermal development region with axial conduction, Wärme-und Stoffübertragung 1 (3) (1968) 177–184.

[23] R. K. Shah, A. L. London, Laminar flow forced convection in ducts: a source book for compact heat exchanger analytical data, Academic press, 2014.

[24] D. Nield, A. Kuznetsov, M. Xiong, Thermally developing forced convection in a porous medium: parallel plate channel with walls at uniform temperature, with axial conduction and viscous dissipation effects, International Journal of Heat and Mass Transfer 46 (4) (2003) 643–651.

[25] G. Hetsroni, A. Mosyak, E. Pogrebnyak, L. Yarin, Heat transfer in micro-channels: Comparison of experiments with theory and numerical results, International Journal of Heat and Mass Transfer 48 (25-26) (2005) 5580–5601.

[26] H.-E. Jeong, J.-T. Jeong, Extended graetz problem including streamwise conduction and viscous dissipation in microchannel, International Journal of Heat and Mass Transfer 49 (13-14) (2006) 2151–2157.

[27] B. Cetin, A. G. Yazicioglu, S. Kakac, Fluid flow in microtubes with axial conduction including rarefaction and viscous dissipation, International Communications in Heat and Mass Transfer 35 (5) (2008) 535–544.

[28] F. Verhoff, A numerical solution of the graetz problem with axial conduction included, Laminar Gravity-Flow Film Condensation of Binary Vapor Mixtures of Immiscible Liquids.

[29] G. Yang, M. Ebadian, Thermal radiation and laminar forced convection in the entrace region of a pipe with axial conduction and radiation, International journal of heat and fluid flow 12 (3) (1991) 202–209.

[30] M. Barışık, A. G. Yazıcıoğlu, B. Çetin, S. Kakaç, Analytical solution of thermally developing microtube heat transfer including axial conduction, viscous dissipation, and rarefaction effects, International Communications in Heat and Mass Transfer 67 (2015) 81–88.

[31] Y. Haddout, J. Lahjomri, The extended graetz problem for a gaseous slip flow in micropipe and parallel-plate microchannel with heating section of finite length: Effects of axial conduction, viscous dissipation and pressure work, International Journal of Heat and Mass Transfer 80 (2015) 673–687.

[32] E. H. Kennard, Kinetic theory of gases, with an introduction to statistical mechanics, (1938).

[33] W. M. Deen, Analysis of Transport Phenomena, Topics in Chemical Engineering, Vol. 3.

[34] F. E. Larrodé, C. Housiadas, Y. Drossinos, Slip-flow heat transfer in circular tubes, International Journal of Heat and Mass Transfer 43 (15) (2000) 2669–2680.

[35] K. Horiuchi, P. Dutta, A. Hossain, Joule-heating effects in mixed electroosmotic and pressure-driven microflows under constant wall heat flux, Journal of Engineering Mathematics 54 (2) (2006) 159.

[36] P. Dutta, K. Horiuchi, H.-M. Yin, Thermal characteristics of mixed electroosmotic and pressure-driven microflows, Computers & Mathematics with Applications 52 (5) (2006) 651–670.

[37] G. B. Arfken, H. J. Weber, F. E. Harris, Mathematical Methods for Physicists: A Comprehensive Guide, Academic Press, 2011.

[38] G. Hetsroni, A. Mosyak, E. Pogrebnyak, L. Yarin, Fluid flow in micro-channels, International Journal of Heat and Mass Transfer 48 (10) (2005) 1982–1998.

[39] L. Yarin, A. Mosyak, G. Hetsroni, Fluid flow, heat transfer and boiling in micro-channels, Springer Science & Business Media, 2008.

[40] S. Kandlikar, S. Garimella, D. Li, S. Colin, M. R. King, Heat transfer and fluid flow in minichannels and microchannels, elsevier, 2005.

[41] S. Ge, Y. Gu, M. Chen, A molecular dynamics simulation on the convective heat transfer in nanochannels, Molecular Physics 113 (7) (2015) 703–710.